Optimum configuration of shell-and-tube heat exchangers for the use in low-temperature organic Rankine cycles[☆]

Daniël Walraven[a,c], Ben Laenen[b,c], William D'haeseleer[a,c,*]

[a] *University of Leuven (KU Leuven) Energy Institute - TME branch (Applied Mechanics and Energy Conversion), Celestijnenlaan 300A box 2421, B-3001 Leuven, Belgium*
[b] *Flemish Institute for Technological Research (VITO), Boeretang 200, B-2400 Mol, Belgium*
[c] *EnergyVille (joint venture of VITO and KU Leuven), Dennenstraat 7, B-3600 Genk, Belgium*

Abstract

In this paper, a first step towards a system optimization of organic Rankine cycles (ORCs) is taken by optimizing the cycle parameters together with the configuration of shell-and-tube heat exchangers. In this way every heat exchanger has the optimum allocation of heat-exchanger surface, pressure drop and pinch-point-temperature difference for the given boundary conditions. Different tube configurations are investigated in this paper. It is concluded that the 30°-tube configurations should be used for the single-phase heat exchangers and the 60°-tube configuration for the two-phase heat exchangers. The performance of subcritical cycles can be strongly improved by adding a second pressure level. Recuperated cycles are only useful when the temperature of the heat source after the ORC should be relatively high.

Keywords: ORC, Shell-and-tube heat exchanger, System optimization

1. Introduction

The amount of energy stored in low-temperature geothermal heat sources is huge [1] but the conversion to electricity is inefficient due to the low temperature. Much research has been performed to maximize this conversion efficiency by the use of organic Rankine cycles (ORC) [2–5]. Most of these studies optimize the cycle parameters (pressures, temperatures and mass flow rates) for different working fluids, but make simplifying assumptions about the components. Heat exchangers are assumed to be ideal or to have a fixed pressure drop, pinch-point temperature differences are assumed to be fixed, etc. The choice of these parameters has an important influence on the performance of the ORC and on the total cost of the installation.

Many authors have already investigated the optimal configuration of shell-and-tube heat exchangers [6–9], plate heat exchangers [10, 11], cooling systems [12–14], etc, but mostly independently of the thermodynamic cycle in which they are supposed to operate. When optimizing components, assumptions have to be made about the system in which the components will work (e.g. maximum allowed pressure drop). To avoid non-optimal assumptions, it is best to optimize the cycle and the components together and to perform a full system optimization. In this way, all components are adjusted to each other and to the cycle.

This issue is already touched upon in the literature. The influence of heat exchangers on the cycle was investigated by Madhawa Hettiarachchi et al. [15]. They minimized the ratio of the total heat-exchanger surface and the net electrical power produced by the cycle. The configuration of the heat exchangers was

[☆] Published version: http://dx.doi.org/10.1016/j.enconman.2014.03.066
[*] Corresponding author. Tel.: +32 16 32 25 11; fax: +32 16 32 29 85.
Email addresses: Daniel.Walraven@mech.kuleuven.be (Daniël Walraven), Ben.Laenen@vito.be (Ben Laenen), William.Dhaeseleer@mech.kuleuven.be (William D'haeseleer)

fixed. Franco and Villani [16] divided the ORC in two levels: the system level and the component level. First, the authors optimized the system level. In a next step, they used this optimum system configuration to find the optimal configuration of the components. An iteration between both levels was needed to come to the final solution. The optimal system configuration obtained this way will probably be very close to the one in the first iteration.

In this paper, a first step towards a system optimization of an ORC is taken by including shell-and-tube heat exchangers in the optimization. The shell-and-tube heat exchangers are modeled with the Bell-Delaware method [17, 18], which is a mature model and can be used for single-phase flow, condensing and evaporation. The shell-and-tube heat-exchanger model is added to a previously developed ORC model [4] in which the heat exchangers were assumed to be ideal.

2. Organic Rankine cycle

In this paper, different types of organic Rankine cycles are simulated. They can be of the simple or recuperated type, be subcritical or transcritical and can have one or two pressure levels. Figure 1a shows the scheme of a single-pressure, recuperated ORC. The liquid working fluid is first pumped to a high pressure (1→2), heated by the heat source in the recuperator (2→3), in the economizer (3→4), in the evaporator (4→5) and in the superheater (5→6). Then the working fluid is expanded in the turbine (6→7), cooled in the recuperator (7→8), in the desuperheater (8→9) and in the condenser (9→1). Not all heat exchangers are necessary in all circumstances. Dry fluids, wet fluids and transcritical fluids often do not need a superheater, desuperheater or evaporator, respectively. A simple ORC is obtained by omitting the recuperator in figure 1a.

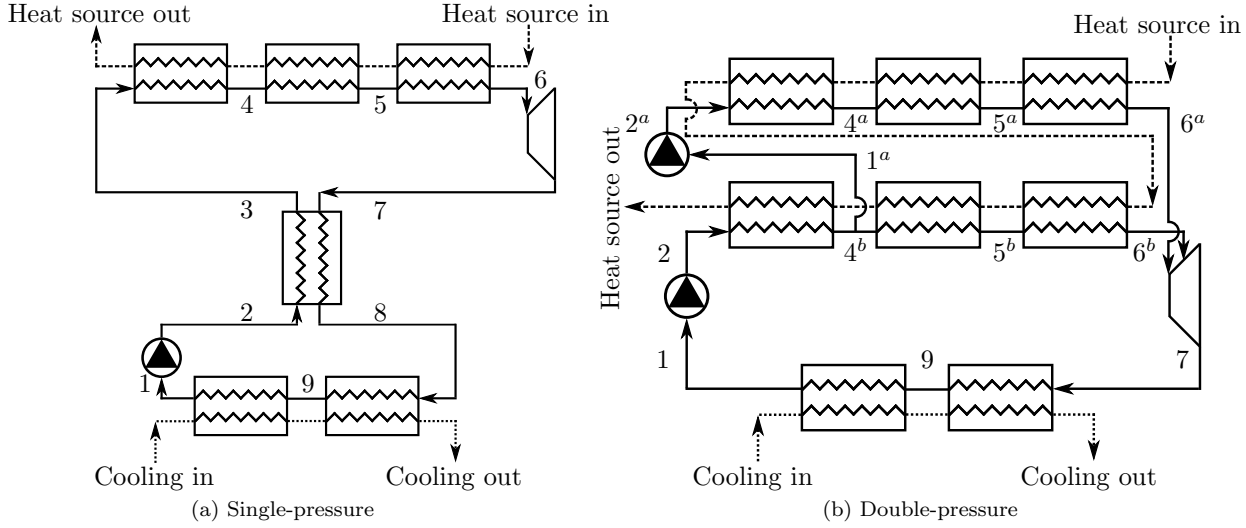

(a) Single-pressure (b) Double-pressure

Figure 1: Scheme of a single-pressure, recuperated (a) and double-pressure, simple (b) ORC.

Figure 1b shows the scheme of a double-pressure, simple ORC. The liquid working fluid is first pumped to an intermediate pressure (1→2) and heated in the intermediate pressure economizer ($2 \rightarrow 1^a/4^b$). A part of the working fluid remains at the intermediate pressure and is heated in the intermediate pressure evaporator ($4^b \rightarrow 5^b$) and superheater ($5^b \rightarrow 6^b$). The other part is pumped to a high pressure ($1^a \rightarrow 2^a$), heated in the high pressure economizer ($2^a \rightarrow 4^a$), evaporator ($4^a \rightarrow 5^a$) and superheater ($5^a \rightarrow 6^a$). Both state 6^a and 6^b are expanded in the turbine ($6^a/6^b \rightarrow 7$) and afterward cooled in the desuperheater (7→9) and in the condenser (9→1). In the case of a double-pressure, recuperated ORC, a recuperator is used which cools down state 7 and heats up state 2, analogous to the single-pressure case.

In all configurations it is assumed that state 1 is saturated liquid and that the isentropic efficiencies of the pump and turbine are 80 and 85%, respectively. More information on the ORC model can be found in Walraven et al. [4], on which this work is based. Instead of assuming a fixed pinch-point temperature difference and ideal heat exchangers, models are used to calculate the heat transfer coefficients and pressure drops in each heat exchanger. These models are described in the following sections. The cycle and components are optimized together in order to maximize the electricity production from a given heat source.

3. Shell-and-tube heat exchanger

3.1. Geometry

Shell-and-tube heat exchangers can be constructed with many different configurations. In this paper it is chosen to only investigate the TEMA E type. This is the most basic type, with a single shell pass and with the inlet and the outlet at the opposite ends of the shell. The working fluid always flows on the shellside, so models for the pressure drop and heat transfer coefficient in single-phase flow, evaporation and condensation in a TEMA E shell are needed. The tube-side fluid (the heat source and heat sink) will always be single phase.

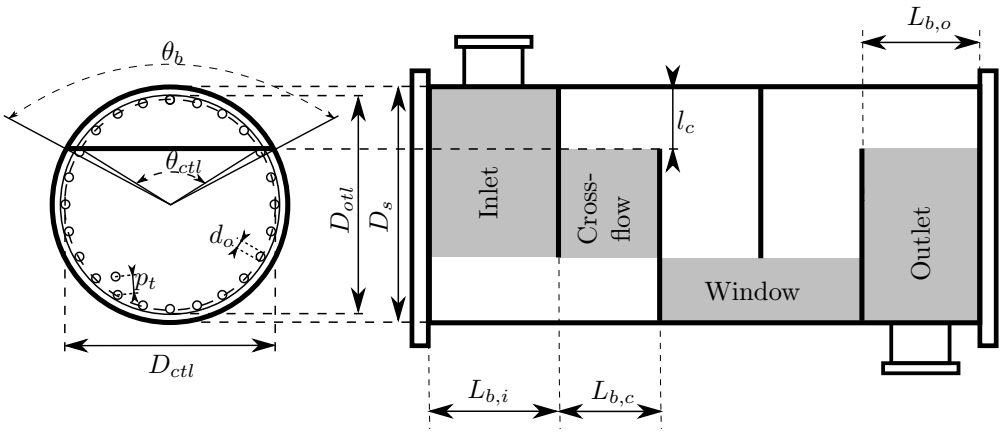

Figure 2: Shell-and-tube geometrical characteristics. Figure adapted from Shah and Sekulić [18].

Figure 2 shows the basic geometrical characteristics of a shell-and-tube heat exchanger. These are the shell outside diameter D_s, the outside diameter of a tube d_o, the pitch between the tubes p_t, the baffle cut length l_c and the baffle spacing at the inlet $L_{b,i}$, outlet $L_{b,o}$ and the center $L_{b,c}$. The expressions to calculate other geometrical characteristics are given in Appendix A, which can also be found in the literature [17, 18]. The inlet, the outlet, a crossflow and a window section are also indicated on figure 2.

3.2. Bell-Delaware

The Bell-Delaware method [17, 18], which is based on the reasoning of Tinker [19], is used to calculate the pressure drop and heat-transfer coefficient on the shellside. Tinker [19] divided the flow in the shell in a number of streams, as shown in figure 3:

- Stream B: ideal crossflow stream
- Stream A: tube-to-baffle hole leakage stream
- Stream C: bundle-to-shell bypass stream
- Stream E: shell-to-baffle leakage stream

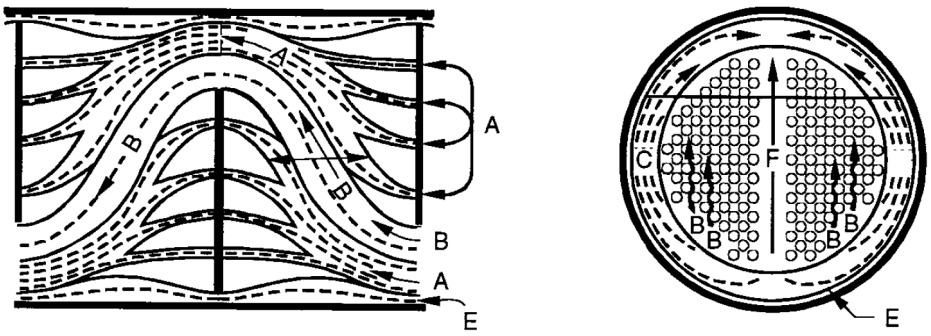

Figure 3: Shell-side flow distribution and different streams. Figure from Shah and Sekulić [18].

- Stream F: tube-pass bypass stream

The shell-side heat-transfer coefficient is given as:

$$h_s = h_{id} J_c J_l J_b J_s J_r, \tag{1}$$

with h_{id} the ideal heat-transfer coefficient for cross flow over a tube bundle and J_x correction factors for non-idealities:

- J_c: correction factor for baffle configuration, given by $J_c = 0.55 + 0.72F_c$
- J_l: correction factor for baffle leakage, given by $J_l = 0.44(1 - r_s) + [1 - 0.44(1 - r_s)]e^{-2.2r_{lm}}$ with $r_s = \frac{A_{o,sb}}{A_{o,sb}+A_{o,tb}}$ and $r_{lm} = \frac{A_{o,sb}+A_{o,tb}}{A_{o,cr}}$
- J_b: correction factor for bundle and pass partition bypass. In this paper it is assumed that enough sealing strips are available, so that $J_b = 1$.
- J_s: correction factor for larger baffle spacing at the inlet and outlet. In this paper it is assumed that $L_{b,i} = L_{b,o} = L_{b,c}$, so that $J_s = 1$.
- J_r: correction factor for an adverse temperature gradient in laminar flow. This effect is neglected in this paper because it normally does not occur in optimized heat exchangers and to avoid numerical issues.

The shell-side frictional pressure drop is given as:

$$[\Delta p_s]_{fr} = [\Delta p_{cr}]_{fr} + [\Delta p_w]_{fr} + [\Delta p_{i-o}]_{fr}, \tag{2}$$

$$= \{(N_b - 1)[\Delta p_{b,id}]_{fr}\zeta_b + N_b[\Delta p_{w,id}]_{fr}\}\,\zeta_l + 2[\Delta p_{b,id}]_{fr}\left(1 + \frac{N_{r,cw}}{N_{r,cc}}\right)\zeta_b\zeta_s, \tag{3}$$

where $[\Delta p_{cr}]_{fr}$, $[\Delta p_w]_{fr}$ and $[\Delta p_{i-o}]_{fr}$ are the frictional pressure drops in the crossflow, window and inlet-outlet sections, respectively. $[\Delta p_{b,id}]_{fr}$ and $[\Delta p_{w,id}]_{fr}$ are the ideal frictional pressure drops in crossflow and window flow, respectively. N_b is the number of baffles, $N_{r,cw}$ and $N_{r,cc}$ the effective number of rows crossed in one window flow and one cross flow, respectively. ζ_x is a correction factor for non-idealities:

- ζ_l: correction factor for baffle leakage, given by $\zeta_l = \exp\left[-1.33(1 + r_s)r_{lm}^p\right]$ with $p = [-0.15(1 + r_s) + 0.8]$
- ζ_b: correction factor for bypass flow. In this paper it is assumed that enough sealing strips are used, so that $\zeta_b = 1$.
- ζ_s: correction factor for larger baffle spacing at the inlet and outlet. In this paper, all baffle spacings are assumed to be equal, so that $\zeta_s = 1$.

3.3. Ideal heat transfer and pressure drop

To apply the Bell-Delaware method, the ideal heat-transfer coefficient and the ideal pressure drops in the cross flow and window flow section are needed. Correlations for these parameters are given in Appendix B for single-phase flow, condensation and evaporation in the shell, together with correlations for single-phase flow on the tube side, which can also be found in the literature [17, 18].

3.4. Implementation of the models

To account for non-uniform fluid properties, each heat exchanger is divided into five parts with an equal heat load[1]. This number is chosen because it leads to a reasonable accuracy and calculation time. For each heat exchanger, the configuration (D_s, d_o, p_t, l_c and $L_{b,c}$), the inlet states at one side of the heat exchanger and a necessary outlet condition (e.g. the working fluid has to be saturated vapor at the end of the evaporator) are needed. With these data, the total heat that has to be transferred in the case of no pressure drop can be calculated. In each of the five parts one fifth of the total heat will be exchanged. With the equations above, the heat-transfer coefficient and the pressure drop in the first part can be calculated. In this way, the state after the first part, the necessary heat-transfer surface and the fictive tube length of the first part L_1 can be calculated. This procedure is repeated for the other parts, except in the last part for which the heat to be transferred is corrected for the pressure drop in the previous parts.

The problem which occurs in this procedure is that the frictional pressure drop in the cross-flow section is different from the one in the window section, while the heat-transfer coefficient is an average of both sections. Therefore it is chosen to average the frictional pressure drop in each section:

$$[\Delta p_s^{parts\ 1,5}]_{fr} = \left\{ \frac{L_i}{L_{b,c}} [\Delta p_{b,id}]_{fr} \zeta_b + \left(\frac{L_i}{L_{b,c}} - \frac{1}{5} \right) [\Delta p_{w,id}]_{fr} \right\} \zeta_l + [\Delta p_{b,id}]_{fr} \frac{N_{r,cw}}{N_{r,cc}} \zeta_b \zeta_s, \tag{4}$$

$$[\Delta p_s^{parts\ 2,3,4}]_{fr} = \left\{ \frac{L_i}{L_{b,c}} [\Delta p_{b,id}]_{fr} \zeta_b + \left(\frac{L_i}{L_{b,c}} - \frac{1}{5} \right) [\Delta p_{w,id}]_{fr} \right\} \zeta_l, \tag{5}$$

with L_i the fictive length of ith part. Addition of these pressure drops for the different parts, leads again to equation (3) when taking into account that $N_b = \sum_i L_i / L_{b,c} - 1$.

4. Optimization

4.1. Objective function

The goal of the optimization is to find a system configuration which maximizes the mechanical work output for a given heat source. This is the same as maximizing the exergetic plant efficiency [4], defined as:

$$\eta_{ex}^{plant} = \frac{\dot{W}_{net}}{\dot{m}^{source} e_{in}^{source}} \tag{6}$$

with $\dot{W}_{net}$ the net mechanical-power production of the power plant, $\dot{m}^{source}$ the mass flow of the source and e_{in}^{source} the flow exergy of the source.

[1] These parts generally do not have the same physical size.

4.2. Optimization variables and constraints

The optimization variables which determine the cycle configuration in a single-pressure, simple cycle are the temperature and pressure before the turbine T_6 and p_6, the mass flow of working fluid $\dot{m}_{wf}$ and the temperature after the condenser T_1. Instead of using p_6 as an optimization variable, the saturation temperature $T^{sat}(p_6)$ is used. In this way linear constraints are obtained between the optimization variables instead of non-linear ones. For a recuperated cycle, the temperature difference between states 2 and 8 is added as an optimization variable. For a double-pressure cycle, T_6^b, $T^{sat}(p_6^b)$ and $\dot{m}_{wf}^b$ are added as optimization variables. State 6 should always be saturated or superheated vapor and T_1 should be the lowest temperature in the ORC. To avoid numerical problems, a minimum superheating of state 6 with 1°C is imposed.[2]

The optimization variables and constraints imposed for each shell-and-tube heat exchanger are given in table 1.

Optimization variable	Lower boundary	Upper boundary
Shell diameter D_s	0.3 m	2 m
Tube outside diameter d_o	5 mm	50 mm
Relative tube pitch p_t/d_o	1.15	2.5
Relative baffle cut l_c/D_s	0.25	0.45
Baffle spacing $L_{b,c}$	0.3 m	5 m
Ratio of tube diameter to shell diameter d_o/D_s	/	0.1

Table 1: Optimization variables and constraints used for shell-and-tube heat exchangers and their lower and upper boundaries.

If no constraint on the heat-exchanger surface of each heat exchanger is imposed, the pinch-point temperature differences would become very small and the total heat-exchanger surface would become huge. Therefore, a non-linear constraint[3] on the total heat-exchanger surface of all heat exchangers together A^{tot} is imposed: $A^{tot} \leq A^{tot}_{max}$. In this way, the optimizer can choose itself how to distribute the available surface optimally amongst the different heat exchangers.

A last constraint is a limit on the heat-source outlet temperature. In some circumstances, the heat-source outlet temperature cannot be too low, e.g. to use the heat source for heating or to avoid scaling with geothermal brines. This is again a non-linear constraint: $T^{source}_{out} \geq T^{source}_{min}$.

A gradient-based optimization method is used to find the optimal system configuration. However calculation of the gradient of the objective function and non-linear constraints with finite-differences gives two problems:

- Slow calculation time: the calculation time is directly proportional the number of optimization variables
- Low accuracy: an inaccurate gradient results in a higher number of iterations

To avoid these issues, the gradients are calculated with automatic differentiation in reverse/adjoint mode. Following this method, the calculation time is independent of the number of optimization variables and the method is accurate up to machine precision.

The ORC and shell-and-tube models are self-written in Python and the CasADi software [20] is used for the optimization. CasADi is a symbolic framework for automatic differentiation and numeric optimization, which can calculate the gradient of the Python-code with automatic differentiation. Many optimizers can

[2]This can have a small, negative influence on the performance of cycles with dry fluids.
[3]The total heat-exchangers surface is a result of the program and the constraint is therefore non linear.

be connected to CasADi, but the one used in this paper is WORHP [21].

The fluid properties are obtained from REFPROP [22]. CasADi also needs the derivative of the fluid properties to calculate the gradient of the objective function and constraints. Therefore the REFPROP fortran code is adapted; the complex-step derivative method [23] is used to obtain the derivative of the fluid properties. The connection between fortran and Python is made by F2PY [24]. A flow chart which shows the connection between the different software packages is shown in figure 4.

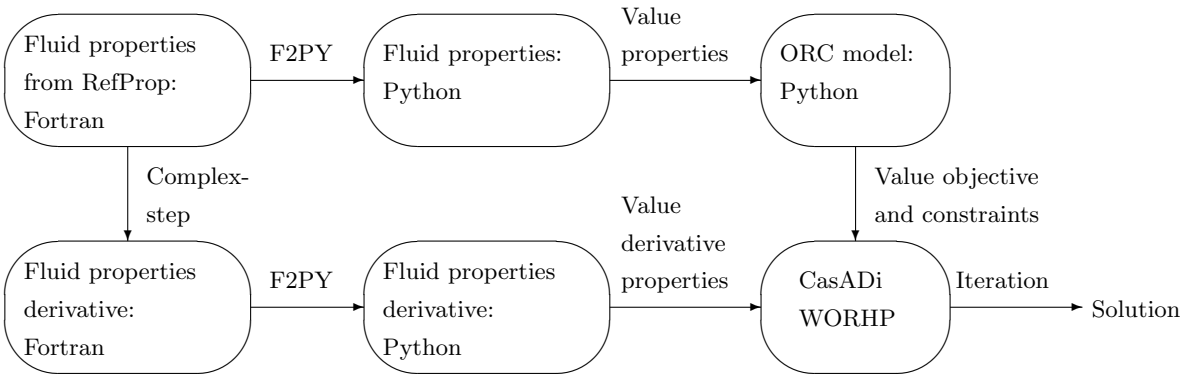

Figure 4: Flow chart showing the connection between the different software packages.

4.3. Advantage system optimization

Instead of a system optimization, it would also be possible to perform an iteration between the optimization of the system level and the component level as performed by Franco and Villani [16]. First the system level is optimized, while making a guess for the optimal value of the pressure drop and the pinch-point-temperature differences. Afterward the heat exchanger surface of each exchanger is minimized separately, while respecting the load of each heat exchanger. This results in new values of the pressure drop, so that an iteration between the system level and the component level is necessary. The results of this method are the power output and the heat exchanger surface of each heat exchanger for the given pinch-point-temperature differences. It is possible that a cycle with other values of the pinch-point-temperature differences produces more electricity for the same total heat exchanger surface and the obtained result is therefore not necessarily a global optimum. So, it is necessary to vary the value of these pinch-point-temperature differences to obtain the optimal system, which results in large calculation times.

The advantage of the system optimization described in this paper is that the optimal pinch-point-temperature differences are a result of the method, because all components are coupled directly and the optimization solver can choose how to allocate the total heat exchanger surface.

5. Results

5.1. Reference parameters

100 kg/s of water is used as the heat source. The parameters for the reference case are given in table 2.
The values of these parameters have of course a strong influence on the performance and cost of the power plant. The main goal of this paper is to show that a system optimization of an ORC can work and the impact of the reference parameters will be investigated in future work.

5.2. Unconstrained heat source outlet temperature

In this section no limit is imposed on the heat-source outlet temperature. The optimizer can choose the optimal heat-source outlet temperature to maximize the plant efficiency, while respecting the boundary conditions.

Parameter	Symbol	Value
Heat source inlet temperature	T_{in}^{source}	125°C
Maximum allowed heat exchanger surface	A_{max}^{tot}	4000 m^2
Cooling fluid inlet temperature	$T_{in}^{cooling}$	20°C
Cooling fluid mass flow	$\dot{m}^{cooling}$	800 kg/s

Table 2: Reference parameters.

5.2.1. Tube configuration shell-and-tube heat exchangers

In this section the influence of the tube configuration (30, 45, 60 or 90° - See Appendix A for the layout of the tubes) on the performance of an ORC is investigated. Figure 5 shows this influence on the exergetic plant efficiency, the net power output and energetic cycle efficiency for single-pressure, simple ORCs. This cycle efficiency is defined as:

$$\eta_{en}^{cycle} = \frac{\dot{W}_{net}}{\dot{Q}} \tag{7}$$

with $\dot{Q}$ the heat added to the cycle. Five different cases are shown; the first four cases (30, 45, 60 or 90°)

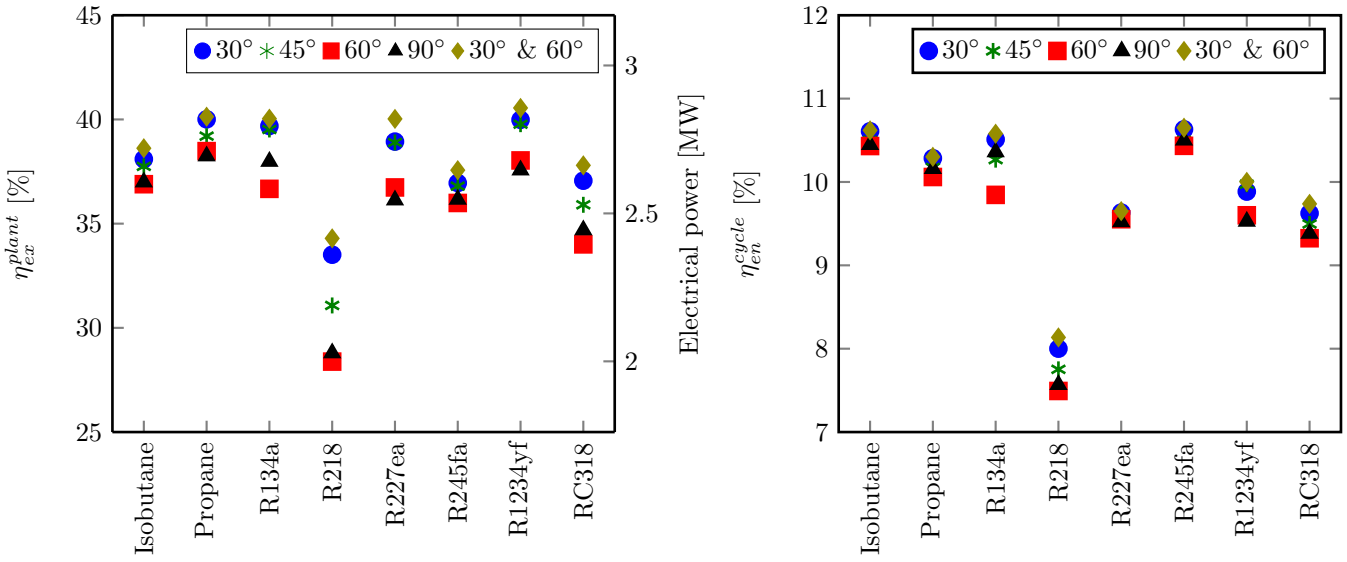

(a) Exergetic plant efficiency

(b) Energetic cycle efficiency

Figure 5: Exergetic plant efficiency and electrical power output (a) and energetic cycle efficiency (b) for single-pressure, simple ORCs with all shell-and-tube heat exchangers for different fluids and different tube configurations. (For the layout of the tubes, see Appendix A.)

have the same tube configuration in all heat exchangers, while the last case uses the 30° configuration in the single-phase heat exchangers (economizer, superheater and desuperheater) and the 60° configuration in the two-phase heat exchangers (evaporator and condenser), which will be called the 30- & 60°-tube configuration in the remainder of this paper. The results show that the 30- & 60°-tube configuration performs the best. 30°- & 60°-tube configuration can combine high heat-transfer coefficients with relatively low pressure drop in single-phase configurations and two-phase flow, respectively [17]. Figure 5a shows that the tube configuration has a very strong effect on the plant performance for transcritical cycles (e.g. R218, R227ea). The cycle with R218 as working fluid and the 30°- & 60°-tube configuration has an exergetic plant efficiency of 34.3%. When using the 60°-tube configuration in all heat exchangers, the plant efficiency decreases to 28.4%. These results show that the configuration of heat exchangers can have a very strong influence on the

performance of an ORC. The energetic cycle efficiency in figure 5b is also influenced by the tube configuration, but not as strong as the plant efficiency. This means that the heat-source outlet temperature decreases too when selecting a "better" tube configuration.

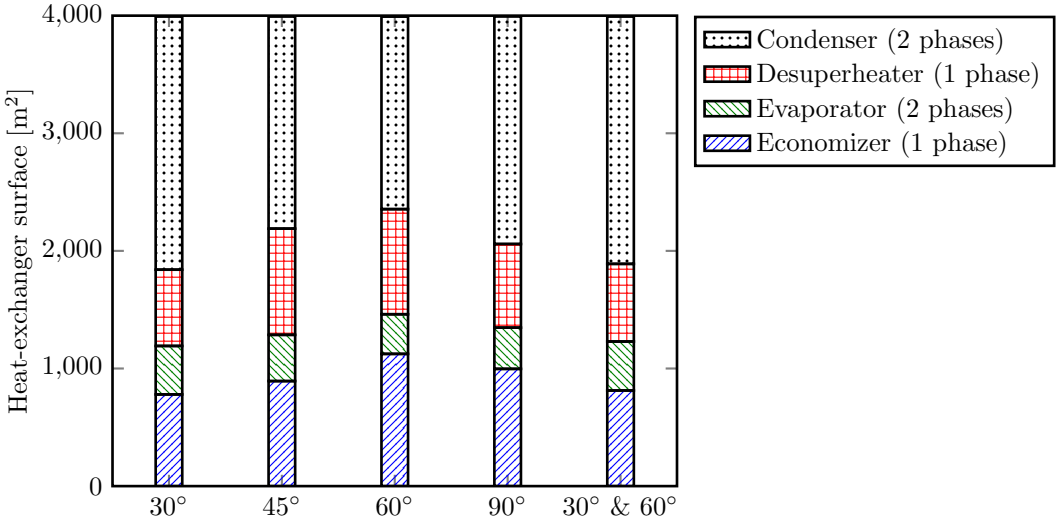

Figure 6: Distribution of the heat-exchanger surface for different tube configurations with isobutane as the working fluid. The surface of the superheater is very small in all cases and is not shown in the figure.

Figure 6 shows the distribution of the heat-exchanger surface amongst the different heat exchangers for the five investigated tube-configurations with isobutane as the working fluid. The 30°-configuration uses a relatively large part of the available surface in the two-phase heat exchangers, while the 60°-configuration on the other hand uses a relatively large part of the surface in the single-phase heat exchangers. The 30°- & 60°-tube configuration results in about the same distribution as in the 30°-case, but leads to smaller pinch-point temperature differences.

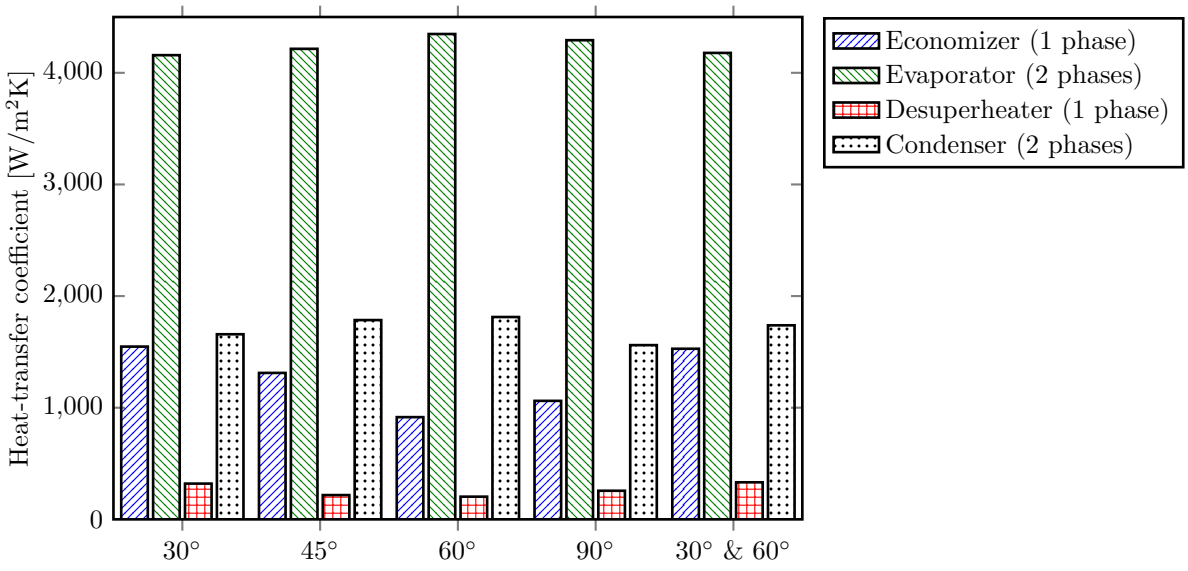

Figure 7: Average heat-transfer coefficient for different tube configurations with isobutane as the working fluid.

The same is seen in figure 7. The 30°-tube configuration and the 60°-tube configuration have the highest

average heat-transfer coefficient in the single-phase heat exchangers and the two-phase heat exchangers, respectively, for isobutane. Combining these two (mono-layout) tube configurations for different heat exchangers results in relatively high heat transfer coefficients in all heat exchangers.

For stand-alone shell-and-tube heat exchangers, it is common practice to select the 30°-tube configuration for the single-phase heat exchangers and to select the 60°-tube configuration for phase-change flow [17, 18]. The foregoing results show that the experience with the tube configuration of stand-alone exchangers is also valid for heat exchangers in an ORC.

The 30°- & 60°-tube configuration performs the best for all fluids and will be used in the remainder of this paper.

Figure 8 shows the exergetic plant, the net power output and energetic cycle efficiency for single- and double-pressure ORCs. Both use the 30°-tube configuration and the 60°-tube configuration for the single-phase and two-phase heat exchangers, respectively. The plant efficiency of subcritical cycles (isobutane, propane, R134a, R245fa and RC318) can increase strongly by adding a second pressure level. The extra pressure level has a limited effect for transcritical cycles. These transcritical cycles are outperformed by the dual-pressure subcritical ones.

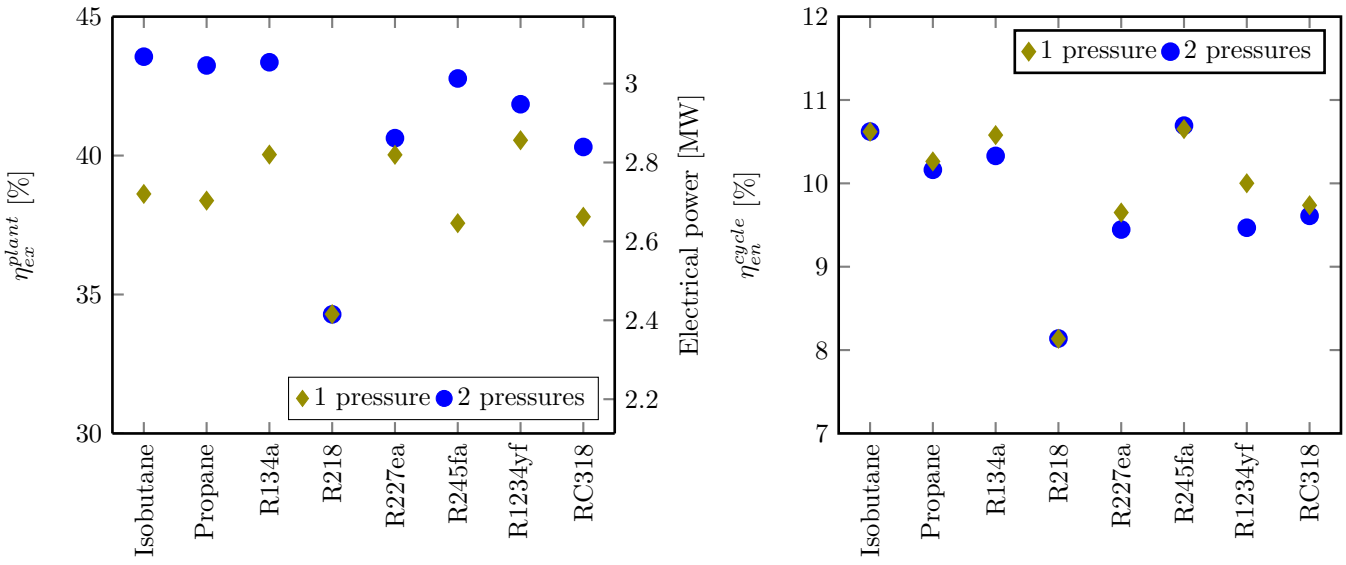

(a) Exergetic plant efficiency

(b) Energetic cycle efficiency

Figure 8: Exergetic plant efficiency and electrical power output (a) and energetic cycle efficiency (b) for single-pressure and double-pressure, simple ORCs with all shell-and-tube heat exchangers for different fluids. Single-phase heat exchangers use the 30°-tube configuration and the two-phase heat exchangers use the 60°-tube configuration.

The energetic cycle efficiency (see figure 8b) does not increase or even decreases by adding an extra pressure level. This means that the increase of the plant efficiency results from a decrease in the heat-source outlet temperature, which is seen in figure 9. The outlet temperature can decrease almost 10°C for subcritical cycles, while the decrease is limited for transcritical cycles.

5.3. Constrained heat-source outlet temperature

It is possible to use the heat source for both electricity production and useful heat delivery. When a series configuration is used, the temperature of the heat source after the ORC has to be warm enough to deliver the

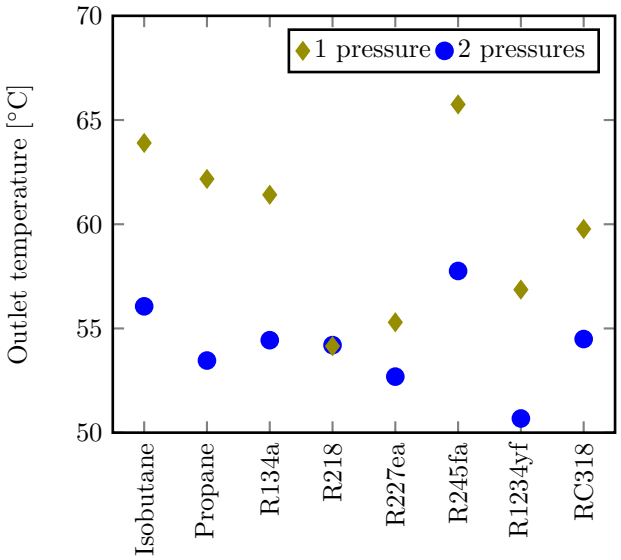

Figure 9: Heat-source outlet temperature for single-pressure and double-pressure simple ORCs with all shell-and-tube heat exchangers for different fluids. The transcritical cycles are the ones with R218, R227ea and R1234yf.

heat. In this section the heat-source outlet temperature is constrained and the influence on the performance of the power plant is investigated.

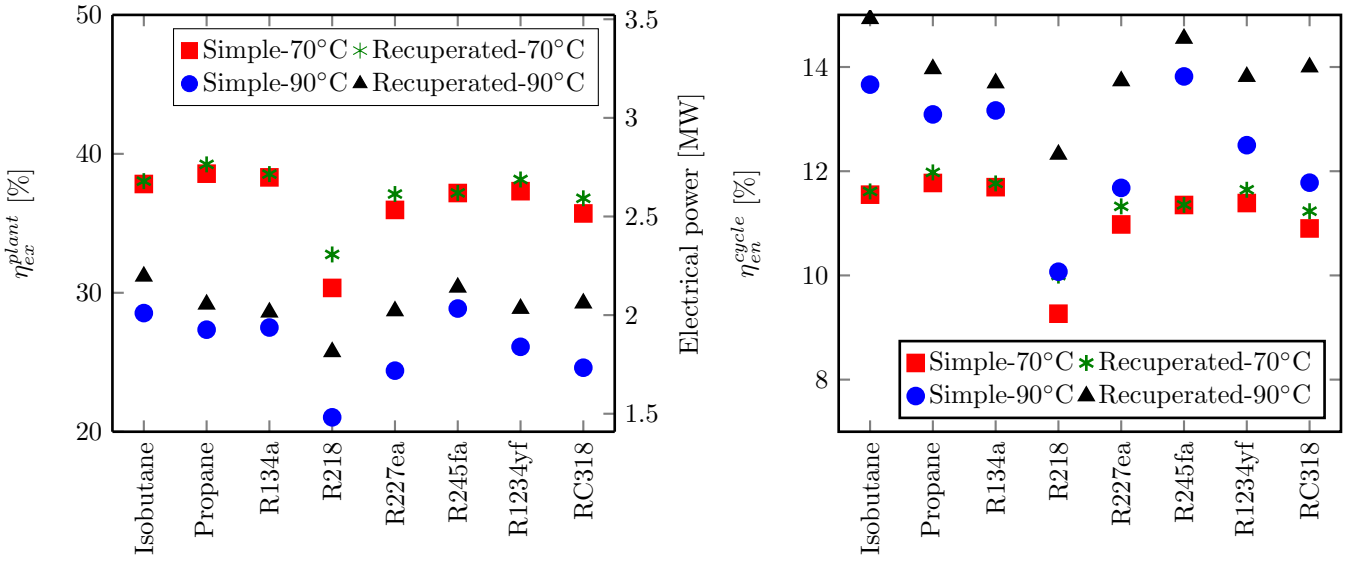

(a) Exergetic plant efficiency

(b) Energetic cycle efficiency

Figure 10: Exergetic plant efficiency and electrical power output (a) and energetic cycle efficiency (b) for single-pressure, simple and recuperated ORCs with all shell-and-tube heat exchangers for different fluids. The heat source outlet temperature is constained to 70 or 90°C.

Figure 10a shows the exergetic plant efficiency and net power output for both simple and recuperated cycles when the minimum heat-source outlet temperature is 70 or 90°C. The plant efficiency increases in most cases by adding a recuperator. The higher the required heat source outlet temperature, the higher is

the effect of the recuperator. The plant efficiency is of course higher when the constraint on the heat source outlet temperature is lower.

Because of the internal heat recuperation in the recuperated cycle, less heat is added to the cycle and the cycle efficiency is higher than in the simple cycle. This is seen in figure 10b. When the heat source outlet temperature is limited to 90°C, the cycle efficiency is (much) higher than in the case of a 70°C-limit for both the simple and recuperated cycle. When the heat source outlet temperature increases, the heat source cooling efficiency decreases and the optimizer chooses to increase the cycle efficiency in order to limit the decrease of the plant efficiency.

6. Conclusions

The system optimization of different configurations of ORCs with shell-and-tube heat exchangers is performed in this paper. Models for heat exchangers used in single-phase flow, evaporation and condensation which are available in the literature are implemented and added to a previously developed ORC-model. The configuration of all heat exchangers and the cycle parameters are optimized together. The total heat-exchanger surface of all heat exchangers together is constrained in order to avoid an unrealistically large and expensive power plant.

Five different tube configurations are compared to each other. If all heat exchangers should have the same tube configuration, it is best to use the 30°-tube configuration. An efficiency improvement can be obtained by applying the 30°-tube configuration and the 60°-tube configurations in the single-phase and two-phase heat exchangers, respectively.

The plant efficiency of subcritical, single-pressure cycles can increase strongly by adding a second pressure level. This increase is induced by a decrease of the heat-source outlet temperature. The cycle efficiency remains about constant.

It is also shown that recuperated cycles are only useful when the heat-source outlet temperature is constrained. The higher the heat-source outlet temperature has to be, the higher the effect of recuperation. An increase in the heat-source outlet temperature results, both for simple and recuperated cycles, in a higher cycle efficiency. Due to the constraint on the heat-source outlet temperature, the heat-source cooling efficiency is limited and the only way to adapt the plant efficiency is by adapting the cycle efficiency.

Future steps in this research will be to include more components and to go towards an economic system optimization.

Nomenclature

Greek

δ	Clearance [m]
Δp	Pressure drop [Pa]
ΔT	Temperature difference [°C]
η	Efficiency [-]
μ	Dynamic viscosity [Pa s]
ρ	Density [kg/m^3]
θ	Angle [°]
ζ	Correction factor for non-ideality in pressure drop [-]

Roman

A	Area [m^2]
c_p	Specific eat capacity [J/kgK]
d_o	Tube outside diameter [m]
D	Diameter [m]
e	Specific exergy [kJ/kg]
F	Fraction of number of tubes [-]
G	Mass velocity [kg/m^2s]
h	Heat transfer coefficient [W/m^2K]
	Specific enthalpy [J/kg]
Hg	Hagen number [-]
J	Correction factor for non-ideality in heat transfer [-]
l_c	Baffle cut length [m]
L_b	Baffle cut length [m]
L_i	Tube length of part i [m]
Lq	Lévêque number [-]
$\dot{m}$	Mass flow [kg/s]
N_b	Number of baffles [-]
N_t	Number of tubes [-]
Nu	Nusselt number [-]
p	Pressure [bar]
Pr	Prandtl number [-]
p_t	Tube pitch [m]
$\dot{Q}$	Heat flow [kW]
Re	Reynolds number [-]
T	Temperature [°C]
$\dot{W}$	Mechanical power [kW]
X	Tube pitch [m]
Y^2	Chisholm parameter [-]

Sub-and superscripts

0	Dead state
$1-9$	Number of the state
ac	Acceleration
c	Center
cr	Crossflow
ctl	Center outermost tubes
$cycle$	Cycle
en	Energetic
ex	Exergetic
fr	Frictional
h	Hydraulic
id	Ideal
in	Inlet
max	Maximum
min	Minimum
net	Nett
l	Longitudinal
otl	Outermost tubes
out	Outlet
$plant$	Plant
s	Shell
$source$	Heat source
t	Transverse
tot	Total
w	Window flow
wf	Working fluid

Acknowledgments

Daniël Walraven is supported by a VITO doctoral grant. The valuable discussions on optimization with Joris Gillis (KU Leuven) are gratefully acknowledged and highly appreciated.

References

[1] J. Tester, B. Anderson, A. Batchelor, D. Blackwell, R. DiPippo, E. Drake, J. Garnish, B. Livesay, M. Moore, K. Nichols, The Future of Geothermal Energy: Impact of Enhanced Geothermal Systems (EGS) on the United States in the 21st Century, Tech. Rep., Massachusetts Institute of Technology, Massachusetts, USA, 2006.

[2] Y. Dai, J. Wang, L. Gao, Parametric optimization and comparative study of organic Rankine cycle (ORC) for low grade waste heat recovery, Energy Conversion and Management 50 (3) (2009) 576–582.

[3] B. Saleh, G. Koglbauer, M. Wendland, J. Fischer, Working fluids for low-temperature organic Rankine cycles, Energy 32 (7) (2007) 1210–1221.

[4] D. Walraven, B. Laenen, W. Dhaeseleer, Comparison of thermodynamic cycles for power production from low-temperature geothermal heat sources, Energy Conversion and Management 66 (2013) 220–233.

[5] D. Wei, X. Lu, Z. Lu, J. Gu, Performance analysis and optimization of organic Rankine cycle (ORC) for waste heat recovery, Energy conversion and Management 48 (4) (2007) 1113–1119.

[6] B. Babu, S. Munawar, Differential evolution strategies for optimal design of shell-and-tube heat exchangers, Chemical Engineering Science 62 (14) (2007) 3720–3739.

[7] B. Allen, L. Gosselin, Optimal geometry and flow arrangement for minimizing the cost of shell-and-tube condensers, International Journal of Energy Research 32 (10) (2008) 958–969.

[8] A. L. Costa, E. M. Queiroz, Design optimization of shell-and-tube heat exchangers, Applied Thermal Engineering 28 (14) (2008) 1798–1805.

[9] V. Patel, R. Rao, Design optimization of shell-and-tube heat exchanger using particle swarm optimization technique, Applied Thermal Engineering 30 (11) (2010) 1417–1425.
[10] L. Wang, B. Sunden, Optimal design of plate heat exchangers with and without pressure drop specifications, Applied Thermal Engineering 23 (3) (2003) 295–311.
[11] J. Zhu, W. Zhang, Optimization design of plate heat exchangers (PHE) for geothermal district heating systems, Geothermics 33 (3) (2004) 337–347.
[12] A. Conradie, J. Buys, D. Kröger, Performance optimization of dry-cooling systems for power plants through SQP methods, Applied thermal engineering 18 (1) (1998) 25–45.
[13] A. Doodman, M. Fesanghary, R. Hosseini, A robust stochastic approach for design optimization of air cooled heat exchangers, Applied Energy 86 (7) (2009) 1240–1245.
[14] E. Rubio-Castro, M. Serna-González, J. M. Ponce-Ortega, M. A. Morales-Cabrera, Optimization of mechanical draft counter flow wet-cooling towers using a rigorous model, Applied Thermal Engineering 31 (16) (2011) 3615–3628.
[15] H. Madhawa Hettiarachchi, M. Golubovic, W. M. Worek, Y. Ikegami, Optimum design criteria for an organic Rankine cycle using low-temperature geothermal heat sources, Energy 32 (9) (2007) 1698–1706.
[16] A. Franco, M. Villani, Optimal design of binary cycle power plants for water-dominated, medium-temperature geothermal fields, Geothermics 38 (4) (2009) 379–391.
[17] G. F. Hewitt, Hemisphere handbook of heat exchanger design, Hemisphere Publishing Corporation New York, 1990.
[18] R. K. Shah, D. P. Sekulić, Fundamentals of heat exchanger design, John Wiley and Sons, Inc., 2003.
[19] T. Tinker, Shell side characteristics of shell and tube heat exchangers, General Discussion on Heat Transfer (1951) 89–116.
[20] J. Andersson, J. Åkesson, M. Diehl, CasADi – A symbolic package for automatic differentiation and optimal control, in: S. Forth, P. Hovland, E. Phipps, J. Utke, A. Walther (Eds.), Recent Advances in Algorithmic Differentiation, vol. 87 of *Lecture Notes in Computational Science and Engineering*, Springer Berlin Heidelberg, 297–307, 2012.
[21] C. Büskens, D. Wassel, The ESA NLP Solver WORHP, in: Modeling and Optimization in Space Engineering, Springer, 85–110, 2013.
[22] E. Lemmon, M. Huber, M. Mclinden, NIST Reference Fluid Thermodynamic and Transport Properties REFPROP, The National Institute of Standards and Technology (NIST), version 8.0, 2007.
[23] J. R. Martins, P. Sturdza, J. J. Alonso, The complex-step derivative approximation, ACM Transactions on Mathematical Software (TOMS) 29 (3) (2003) 245–262.
[24] P. Peterson, F2PY: a tool for connecting Fortran and Python programs, International Journal of Computational Science and Engineering 4 (4) (2009) 296–305.
[25] R. Mukherjee, Effectively design shell-and-tube heat exchangers, Chemical Engineering Progress 94 (2) (1998) 21–37.
[26] B. Petukhov, V. Popov, Theoretical calculation of heat exchange and frictional resistance in turbulent flow in tubes of an incompressible fluid with variable physical properties(Heat exchange and frictional resistance in turbulent flow of liquids with variable physical properties through tubes), High Temperature 1 (1963) 69–83.
[27] M. Bhatti, R. Shah, Turbulent and transition convective heat transfer in ducts, in: S. Kakaç, R. Shah, W. Aung (Eds.), Handbook of Single-Phase Convective Heat Transfer, chap. 4, Wiley, New York, 1987.

Appendix A. Geometry

The equations to calculate the important geometrical parameters of a shell-and-tube heat exchanger are stated in this section. More information can be found in the literature [17, 18], on which this section is based.
The diameter of the outermost tubes D_{otl} and the diameter of the circle through the center of the outermost tubes D_{ctl} are given by:

$$D_{otl} = D_s - \delta_{bb}, \tag{A.1}$$

$$D_{ctl} = D_{otl} - d_o, \tag{A.2}$$

with δ_{bb} the diametrical shell-to-tube bundle bypass clearance, which can be estimated as $\delta_{bb} = 0.017 D_s + 0.0265$ [m] [17]. The remaining two parameters in figure 2 are calculated as:

$$\theta_b = 2\cos^{-1}\left(1 - \frac{2l_c}{D_s}\right), \tag{A.3}$$

$$\theta_{ctl} = 2\cos^{-1}\left(\frac{D_s - 2l_c}{D_{ctl}}\right). \tag{A.4}$$

The number of tubes N_t in a shell without impingement plates and a single tube pass is:

$$N_t = \frac{\pi/4 D_{ctl}^2}{C_t p_t^2}, \tag{A.5}$$

with C_t a constant which depends on the tube bundle configuration. Parameters for the four most used tube bundle configurations as suggested in figure A.1 are given in table A.1.

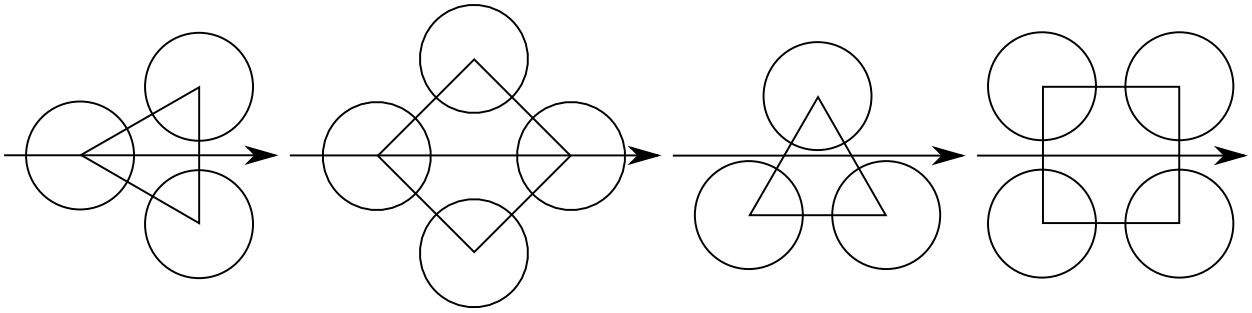

Figure A.1: Tube layout patterns. Figure adapted from Mukherjee [25].

	Staggered array			Inline array
	30°	45°	60°	90°
Transverse tube pitch X_t	p_t	$\sqrt{2}p_t$	$\sqrt{3}p_t$	p_t
Longitudinal tube pitch X_l	$\frac{\sqrt{3}}{2}p_t$	$\frac{p_t}{\sqrt{2}}$	$\frac{p_t}{2}$	p_t
Tube count constant C_t	$\frac{\sqrt{3}}{2}$	1	$\frac{\sqrt{3}}{2}$	1

Table A.1: Geometrical properties of some tube banks. Table adapted from Shah and Sekulić [18].

The gross window area $A_{fr,w}$, the fraction of the number of tubes in one window section F_w, the area occupied by tubes in the window section $A_{fr,t}$, the net flow area in one window section $A_{o,w}$, the hydraulic diameter of the window section $D_{h,w}$ and the number of effective tube rows in crossflow in the window section $N_{r,cw}$ are given by:

$$A_{fr,w} = \frac{D_s^2}{4}\left[\frac{\theta_b}{2} - \left(1 - \frac{2l_c}{D_s}\right)\sin\frac{\theta_b}{2}\right], \tag{A.6}$$

$$F_w = \frac{\theta_{ctl}}{2} - \frac{\sin\theta_{ctl}}{2\pi}, \tag{A.7}$$

$$A_{fr,t} = \frac{\pi}{4}d_o^2 F_w N_t, \tag{A.8}$$

$$A_{o,w} = A_{fr,w} - A_{fr,t}, \tag{A.9}$$

$$D_{h,w} = \frac{4A_{o,w}}{\pi d_o F_w N_t + D_s\theta_b/2}, \tag{A.10}$$

$$N_{r,cw} = \frac{0.8}{X_l}\left[l_c - 0.5(D_s - D_{ctl})\right]. \tag{A.11}$$

The fraction of of the number of tubes in the cross flow section F_c, the number of tube rows crossed in one crossflow section $N_{r,cc}$ and the crossflow area at the shell center line $A_{o,cr}$ can be calculated as:

$$F_c = 1 - 2F_w, \tag{A.12}$$

$$N_{r,cc} = \frac{D_s - 2l_c}{X_l}, \tag{A.13}$$

$$A_{o,cr} = \left[D_s - D_{otl} + \frac{D_{ctl}}{X_t}(X_t - d_o) \right] L_{b,c}, \tag{A.14}$$

$$A_{o,cr} = \left[D_s - D_{otl} + 2\frac{D_{ctl}}{X_t}(p_t - d_o) \right] L_{b,c}. \tag{A.15}$$

The first expression for $A_{o,cr}$ is valid for 30°- and 90°-tube configurations and for 45°- and 60°-tube configurations with a high pitch. The second expression is valid for 45°- and 60°-tube configurations with a low pitch.

The flow area for bypass stream C (section 3.2) F_{bp}, the total tube-to-baffle leakage area for one baffle $A_{o,tb}$ and the shell-to-baffle leakage area $A_{o,sb}$ are given by:

$$F_{bp} = \frac{(D_s - D_{otl})L_{b,c}}{A_{o,cr}}, \tag{A.16}$$

$$A_{o,tb} = \frac{\pi}{4}\left[(d_o + \delta_{tb})^2 - d_o^2\right] N_t(1 - F_w), \tag{A.17}$$

$$A_{o,sb} = \pi D_s \frac{\delta_{sb}}{2}\left(1 - \frac{\theta_b}{2\pi}\right), \tag{A.18}$$

with $\delta_{tb} = 0.4\ 10^{-3}$ [m] the diametrical clearance and $\delta_{sb} = 3.1\ 10^{-3} + 0.004 D_s$ [m] the shell-to-baffle clearance as given by TEMA standards [17].

Appendix B. Heat transfer and pressure drop

B.1. Single-phase flow

B.1.1. Shell side

The ideal heat transfer coefficient on the shell-side in inline tube bundles (90° configurations) is given by [18]:

$$h_{single}^{id,shell} = \frac{k}{D_h} 0.404 Lq^{1/3} \left(\frac{Re_d + 1}{Re_d + 1000} \right)^{0.1}, \tag{B.1}$$

$$Lq = 1.18 Hg\ Pr \left(\frac{(4X_t^*/\pi) - 1}{X_l^*} \right), \tag{B.2}$$

$$Hg = Hg_{lam} + Hg_{turb,i} \left[1 - \exp\left(1 - \frac{Re_d + 1000}{2000} \right) \right], \tag{B.3}$$

$$Hg_{lam} = 140 Re_d \frac{(X_l^{*0.5} - 0.6)^2 + 0.75}{X_t^{*1.6}(4X_t^* X_l^*/\pi - 1)}, \tag{B.4}$$

$$Hg_{turb,i} = \left[\left(0.11 + \frac{0.6(1 - 0.94/X_l^*)^{0.6}}{(X_t^* - 0.85)^{1.3}} \right) 10^{0.47(X_l^*/X_t^* - 1.5)} + 0.015(X_t^* - 1)(X_l^* - 1) \right] \times Re_d^{2 - 0.1(X_l^*/X_t^*)} + \phi_{t,n} Re_d^2, \tag{B.5}$$

$$u_m = u_\infty \frac{X_t^*}{X_t^* - 1}, \tag{B.6}$$

with k the thermal conductivity of the fluid, Lq the Lévêque number, Hg the Hagen number, Pr the Prandtl number, u_∞ the free stream velocity, $\phi_{t,n}$ a correction factor for tube bundle inlet and outlet pressure drops and Re_d the Reynolds number in the shell. These last two parameters are calculated as:

$$\phi_{t,n} = \begin{cases} \frac{1}{2X_t^{*2}}\left(\frac{1}{N_r} - \frac{1}{10}\right) & \text{for } 5 \leq N_r \leq 10 \text{ and } X_l^* \geq 0.5(2X_t^*+1)^{1/2} \\ 2\left[\frac{X_d^*-1}{X_t^*(X_t^*-1)}\right]^2\left(\frac{1}{N_r} - \frac{1}{10}\right) & \text{for } 5 \leq N_r \leq 10 \text{ and } X_l^* < 0.5(2X_t^*+1)^{1/2} \\ 0 & \text{for } N_r > 10 \end{cases}, \tag{B.7}$$

$$Re_d = \frac{\rho u_m d_o}{\mu}. \tag{B.8}$$

X_l^*, X_t^* and X_d^* are dimensionless parameters, obtained by dividing X_l, X_t and $X_d = \sqrt{X_l^2 + X_t^2}$ by d_o, respectively. ρ is the density and μ the dynamic viscosity.
For staggered tube bundles (30, 45 and 60° configurations), the correlations are [18]:

$$h_{single}^{id,shell} = \frac{k}{D_h} 0.404 Lq^{1/3}, \tag{B.9}$$

$$Lq = \begin{cases} 0.92 Hg\ Pr\left(\frac{(4X_t^*/\pi)-1}{X_d^*}\right) & \text{for } X_l^* \geq 1 \\ 0.92 Hg\ Pr\left(\frac{(4X_t^*X_l^*/\pi)-1}{X_l^*X_d^*}\right) & \text{for } X_l^* < 1 \end{cases}, \tag{B.10}$$

$$Hg = Hg_{lam} + Hg_{turb,s}\left[1 - \exp\left(1 - \frac{Re_d + 200}{1000}\right)\right], \tag{B.11}$$

$$Hg_{lam} = \begin{cases} 140 Re_d \frac{(X_l^{*0.5}-0.6)^2+0.75}{X_t^{*1.6}(4X_t^*X_l^*/\pi-1)} & \text{for } X_l^* \geq 0.5(2X_t^2+1)^{1/2} \\ 140 Re_d \frac{(X_l^{*0.5}-0.6)^2+0.75}{X_d^{*1.6}(4X_t^*X_l^*/\pi-1)} & \text{for } X_l^* < 0.5(2X_t^2+1)^{1/2} \end{cases}, \tag{B.12}$$

$$Hg_{turb,s} = \left[\left(1.25 + \frac{0.6}{(X_t^* - 0.85)^{1.08}}\right) + 0.2\left(\frac{X_l^*}{X_t^*} - 1\right)^3 - 0.005\left(\frac{X_t^*}{X_l^*} - 1\right)^3\right] \times Re_d^{1.75} + \phi_{t,n} Re_d^2, \tag{B.13}$$

$$Hg_{turb,s,corr} = Hg_{turb,s}\left(1 + \frac{Re_d - 250\ 000}{325\ 000}\right), \tag{B.14}$$

$$u_m = \begin{cases} u_\infty \frac{X_t^*}{X_t^*-1} & \text{for } X_l^* \geq 0.5(2X_t^*+1)^{1/2} \\ u_\infty \frac{X_t^*}{2(X_d^*-1)} & \text{for } X_l^* < 0.5(2X_t^*+1)^{1/2} \end{cases}. \tag{B.15}$$

The pressure drop in an ideal crossflow section $\Delta p_{b,id}$ between two baffles and in an ideal window flow $\Delta p_{w,id}$ are given by:

$$\Delta p_{b,id} = \frac{\mu^2}{\rho}\frac{N_{r,cc}}{d_o^2} Hg, \tag{B.16}$$

$$\Delta p_{w,id} = \begin{cases} (2 + 0.6 N_{r,cw})\frac{G_w^2}{2\rho} & \text{for } Re_d > 100 \\ \frac{26 G_w \mu}{\rho}\left(\frac{N_{r,cw}}{p_t - d_o} + \frac{L_b}{D_{h,w}^2}\right) + \frac{G_w^2}{\rho} & \text{for } Re_d \leq 100 \end{cases}, \tag{B.17}$$

with G_w the mass velocity in the window section:

$$G_w = \frac{\dot{m}}{\sqrt{A_{o,cr} A_{o,w}}}, \tag{B.18}$$

and $\dot{m}$ the mass flow of the fluid. The hydrostatic pressure drop is neglected because the shell-side fluid flows alternately up and down and the hydrostatic pressure drop is therefore alternately positive and negative. Both are about equal and can therefore be neglected.

B.1.2. Tube side

The correlation of Petukhov and Popov [26] is used to calculate the single phase heat transfer coefficient in the tubes. The friction coefficient is calculated by the correlation of Bhatti and Shah [27].

B.2. Heat transfer and pressure drop while evaporating

The boiling heat transfer coefficient for evaporation on the shell-side is given by [17]:

$$h_{evap}^{id,shell} = h_{nb}F_b + h_{nc}, \tag{B.19}$$

with h_{nb} the nucleate boiling coefficient, F_b a correction factor for the effect of convection and h_{nc} the natural convection heat transfer coefficient, which is about 250 W/m^{2}K for hydrocarbons. The other parameters are given as [17]:

$$h_{nb} = 0.00417 p_{crit}^{0.69} \dot{q}^{0.7} F_p, \tag{B.20}$$

$$F_p = 0.7 + 2p_r \left(4 + \frac{1}{1-p_r}\right), \tag{B.21}$$

$$F_b = 1 + 0.1 \left[\frac{0.785 D_{otl}}{C_t (p_t/d_o)^2 d_o} - 1\right]^{0.75}, \tag{B.22}$$

where p_{crit} is the critical pressure of the fluid, $\dot{q}$ the heat flux and $p_r = p/p_{crit}$ the reduced pressure.
The frictional, ideal pressure drop is given as [17]:

$${}^{fr}\Delta p_{evap}^{id,shell} = \left(1 + (Y^2 - 1)\left[Bx^{(2-n)/2}(1-x)^{(2-n)/2} + x^{2-n}\right]\right)_{lo}^{fr} \Delta p_{single}^{id,shell} \tag{B.23}$$

where ${}_{lo}^{fr}\Delta p_{single}^{shell}$ is the frictional, ideal pressure drop in the shell if all the fluid was saturated liquid, $Y^2 = {}_{lo}^{fr}\Delta p_{id,single}^{shell} / {}_{vo}^{fr}\Delta p_{single}^{id,shell}$ the Chisholm parameter and x the quality of the fluid. For the cross flow $B = 1$ and $n = 0.37$, while for the window flow $B = (\rho_h/\rho_l)^{1/4}$ and $n = 0$. ρ_h is the homogeneous flow density, given as:

$$\rho_h = \frac{1}{\frac{1-x}{\rho_l} + \frac{x}{\rho_v}} \tag{B.24}$$

The subscripts l and v refer to saturated liquid and vapor, respectively.
The acceleration pressure drop is [17]:

$${}^{ac}\Delta p_{evap}^{id,shell} = G^2 \left(\frac{(1-x)^2}{\rho_l(1-\alpha)} + \frac{x^2}{\rho_v \alpha}\right)_{out} - \left(\frac{(1-x)^2}{\rho_l(1-\alpha)} + \frac{x^2}{\rho_v \alpha}\right)_{in}, \tag{B.25}$$

with $\alpha = 1/(1 + \frac{1-x}{x}\frac{\rho_v}{\rho_l})$ the void fraction as calculated for a homogeneous flow [17].

B.3. Heat transfer and pressure drop while condensing

The heat transfer coefficient for condensation on the shell-side is given by [17]:

$$h_{cond}^{id,shell} = \frac{k}{d_o} K \left(\chi^4 Re_{lv}^2 + Nu_f^4\right)^{1/4}, \tag{B.26}$$

with

$$Nu_f^4 = 0.276 \left[\frac{d_o^3 \rho_l (\rho_l - \rho_v) g (h_v - h_l)}{\mu_l k_l (T_{sat} - T_w)} \right], \tag{B.27}$$

$$\chi = 0.9 \left(1 + \frac{1}{RH} \right)^{1/3}, \tag{B.28}$$

$$R = \left(\frac{\rho_l \mu_l}{\rho_g \mu_g} \right)^{1/2}, \tag{B.29}$$

$$H = \frac{c_{p,l}(T_{sat} - T_w)}{Pr_l (h_v - h_l)}, \tag{B.30}$$

$$Re_{lv} = \frac{d_o \frac{\dot{m} x}{L_{bc} D_s} \rho_l}{\mu_l \rho_v}, \tag{B.31}$$

where h is the specific enthalpy and c_p the heat capacity at constant pressure. The two-phase pressure drop is calculated by the same correlations as given for the evaporator.